doi:10.26443/seismica.v5i2.3166

Empirical Relationships Between Ground Motion Intensities and JMA Seismic Intensity Scale

Patrick W. Ball *[1], **Toby Sansom**[1], **Karina Loviknes**[2]

[1]Inigo Insurance Ltd, 25 Fenchurch Avenue, London, United Kingdom, EC3M 5AD, [2]Njord Centre, Department of Physics and Geosciences, University of Oslo, Oslo, Norway

Author contributions: *Conceptualization, Methodology, Formal Analysis & Visualization*: P. Ball. *Data Curation*: P. Ball, K. Loviknes. *Writing - Original draft, Review & Editing*: P. Ball, T. Sansom.

Abstract There is a growing appetite for parametric Japanese earthquake insurance products that use Japanese Meteorological Agency seismic intensity, I_{JMA}, triggers. However, most earthquake risk models used to price these contracts do not compute I_{JMA} directly, instead relying on conversions that introduce additional basis risk. Here, we present empirical parameterisations of I_{JMA} as a function of all combinations of moment magnitude, hypocentral distance, peak ground acceleration (PGA), and spectral acceleration ($S_a(T)$) at 0.2, 0.3, 0.6, 1.0, 2.0, and 3.0 s, derived from earthquake risk model outputs. Parameterisations are fitted using ridge regression applied to 21,354 ground motion recordings from 112 Japanese earthquakes spanning January 1997 to December 2025. A parsimonious three-parameter model — combining PGA, S_a(0.3 s), and S_a(1.0 s) — outperforms a previously published parameterisation, substantially reducing both uncertainty and bias. When applied to a synthetic parametric insurance portfolio exposed to 25 years of Japanese seismicity, this parameterisation yields a measurable reduction in basis risk. These results support more reliable and transparent pricing of parametric earthquake insurance products.

Production Editor: Gareth Funning
Handling Editor: Carmine Galasso
Copy & Layout Editor: Hannah F. Mark

Received: June 8, 2026
Accepted: October 16, 2026
Published: November 4, 2026

Non-technical summary Parametric insurance uses objective thresholds to trigger payouts, rather than calculating exact losses. This speeds up claims settlement, but can create a mismatch between the loss actually suffered and the payment received — known as basis risk. The Shindo Scale measures earthquake shaking intensity and is widely used as a parametric insurance trigger in Japan. However, the earthquake models that insurers use to price these contracts do not directly calculate Shindo Scale values, requiring an additional conversion step. Here, we present improved conversions between earthquake model outputs and the Shindo Scale that substantially reduce basis risk compared to currently available alternatives.

1 Introduction

The Japanese Meteorological Agency (JMA) seismic intensity scale, or Shindo Scale, is a long-established method for categorising the local ground shaking intensity of earthquakes. It was initially devised as a categorical scale, with values assigned by JMA staff based on shaking and damage observations in each location (Hirono and Sato, 1971). In 1996, the JMA transitioned to reporting an instrumentally derived seismic intensity (I_{JMA}) which can be converted to the original Shindo Scale (Table 1; Kiyono et al., 1999; Midorikawa et al., 1999).

The JMA maintains a dense network of three-component ground-motion accelerometers across Japan that record I_{JMA} and Shindo class for all detectable earthquakes. The speed and reliability of JMA reporting coupled with the objectivity of I_{JMA} calculations make Shindo Scale at the nearest observation point an ideal trigger for parametric earthquake insurance in Japan. Parametric, or index-based, insurance utilises predefined hazard thresholds that trigger payouts representing fixed percentages of the total insured limit (Wald and Franco, 2017). Commonly used hazard triggers within parametric earthquake policies include Peak Ground Acceleration (PGA), Modified Mercalli Intensity, and moment magnitude (M_w; Härdle and Cabrera, 2010; Wald and Franco, 2017; Mistry and Lombardi, 2022). These policies can be triggered on a single location and occurrence basis, or they can include additional clauses that consider how losses aggregate across several events and/or properties within a portfolio, with time and distance encompassed by an event strictly defined. Parametric products with JMA Shindo Scale triggers are becoming increasingly popular in Japan since I_{JMA} is strongly tied to building damage and payouts can be delivered in a matter of days after an event (Iwasaki, 2021; Willard, 2025; Descartes Underwriting, 2025).

Both buyers and sellers of parametric products desire contractual terms that seek to minimise the difference between insurance payouts and actual damage incurred, known as basis risk. From the seller's perspective, it is also important to accurately estimate the likelihood that parametric payouts are triggered. Earthquake risk models are commonly utilised by in-

*Corresponding author: patrick.ball@inigoinsurance.com

surers to assess the pricing adequacy of potential deals and manage their exposure to large events (Rao et al., 2025). Hazard calculations within these models generally subdivide into earthquake-frequency and ground-shaking-intensity components. Ground motion intensities are typically parameterised as functions of magnitude, hypocentral distance, fault mechanism and site conditions – and several parameterisations can be used in tandem within a logic tree (e.g., Silva et al., 2020; Fujiwara et al., 2023; Moschetti et al., 2024). Whilst some ground-motion and earthquake-risk models directly estimate I_{JMA} (e.g., Campbell and Bozorgnia, 2011; Earthquake Research Committee, 2021), it is considerably more common to estimate physical parameters such as PGA and spectral acceleration ($S_a(T)$) at several periods (e.g., 0.2 s, 0.3 s, 0.6 s, 1 s, 2 s; Fujiwara et al., 2023). Therefore, most earthquake risk model outputs must be converted into I_{JMA} before they can be used to evaluate the parametric insurance deals described above. This conversion step introduces additional basis risk and frequency uncertainty for parametric insurance proposals with Shindo-Scale triggers.

Published empirical relationships exist between several commonly reported ground motion intensity measures and I_{JMA} (e.g., Karim and Yamazaki, 2002; Fujimoto and Midorikawa, 2010; Pavel and Aldea, 2025). However, these parameterisations all rely on intensity metrics less commonly calculated by ground motion models, e.g., peak ground velocity, spectral intensity, or the max resultant of peak ground acceleration. In some instances, these differences preclude their usage in insurance contexts, while in others additional basis risk is incurred when converting modelled variables into useable formats. Furthermore, these models typically draw upon earthquake datasets limited to 20 or fewer events that occurred prior to 2010. For applications such as parametric property insurance, where only ground shaking exceeding $I_{\text{JMA}} \approx 5.5$ is relevant, incorporating additional strong-motion observations from more recent large events, such as the 2011 Tōhoku-Oki, 2016 Kumamoto, and 2024 Noto earthquakes, should provide improved relationship fitting.

Here, we present new parameterisations for calculating I_{JMA} that can directly leverage ground-motion-model outputs. First, we extract and process a wealth of seismic data from across Japan to calculate I_{JMA} and a suite of ground motion intensity metrics typically provided by ground motion models. Second, we employ a multivariate regression approach to develop relationships between these intensity metrics and I_{JMA}. Third, we test the accuracy of our model using out-of-sample seismic data. Finally, we apply our chosen I_{JMA} parameterisation to a hypothetical parametric insurance portfolio to demonstrate the reduction of basis risk our new approach provides when compared to previously published parameterisations.

2 Extraction and Processing of Seismic Data

The National Research Institute for Earth Science and Disaster Resilience maintain two strong-motion seismographic networks: KiK-net (Kiban-Kyoshin network) and K-Net (Kyoshin network; Aoi et al., 2004, 2010; National Research Institute for Earth Science and Disaster Resilience, 2019). These networks provide dense, ~20 km, coverage across Japan and record three-component waveform data that are made freely available. We extracted ground motion data for 112 earthquakes between January 1997 and December 2025 that are $\geq M_w$ 5.0 and have a recording of ≥ 5.0 I_{JMA} for at least one station (Figure 1a). We only use KiK-net observations from the surface seismometer and all recordings are corrected using scaling factors provided with the data.

I_{JMA} is calculated from three-component acceleration time histories (Kiyono et al., 1999; Midorikawa et al., 1999). First, the acceleration time history in each shaking orientation is transformed into the frequency (f) domain using a Fourier transform. To isolate the range of ground motions associated with perceptible shaking and potential damage, a band-pass filter is applied to each spectra that combines a low-cut, high-cut, and periodic filter (F_{low}, F_{high}, and F_{period}, respectively):

$$
\begin{aligned}
F_{high} &= \sqrt{1 - \exp\left(-\left(\frac{f}{0.5}\right)^3\right)}, \\
F_{low} &= \frac{1}{\sqrt{1 + 0.694\left(\frac{f}{10}\right)^2 + 0.241\left(\frac{f}{10}\right)^4 + 0.0557\left(\frac{f}{10}\right)^6 + 0.009664\left(\frac{f}{10}\right)^8 + 0.00134\left(\frac{f}{10}\right)^{10} + 0.000155\left(\frac{f}{10}\right)^{12}}}, \\
F_{period} &= \sqrt{\frac{1}{f}}.
\end{aligned}
\tag{1}
$$

These filtered spectra are then transformed back into the time domain using an inverse Fourier transform, and combined using a root-sum-square approach into a single accelerogram. From this combined signal, a_0 is taken as the highest acceleration sustained for a minimum cumulative duration of 0.3 s. Finally, I_{JMA} is com-

Instrumental Intensity	Shindo Class	Instrumental Intensity	Shindo Class
$I_{\text{JMA}} < 0.5$	0	$4.5 \leq I_{\text{JMA}} < 5.0$	5 lower (5−)
$0.5 \leq I_{\text{JMA}} < 1.5$	1	$5.0 \leq I_{\text{JMA}} < 5.5$	5 upper (5+)
$1.5 \leq I_{\text{JMA}} < 2.5$	2	$5.5 \leq I_{\text{JMA}} < 6.0$	6 lower (6−)
$2.5 \leq I_{\text{JMA}} < 3.5$	3	$6.0 \leq I_{\text{JMA}} < 6.5$	6 upper (6+)
$3.5 \leq I_{\text{JMA}} < 4.5$	4	$I_{\text{JMA}} \geq 6.5$	7

Table 1 Conversion between Japanese Meteorological Agency (JMA) instrumentally derived seismic intensity (I_{JMA}) and the traditional classification system (Shindo Scale).

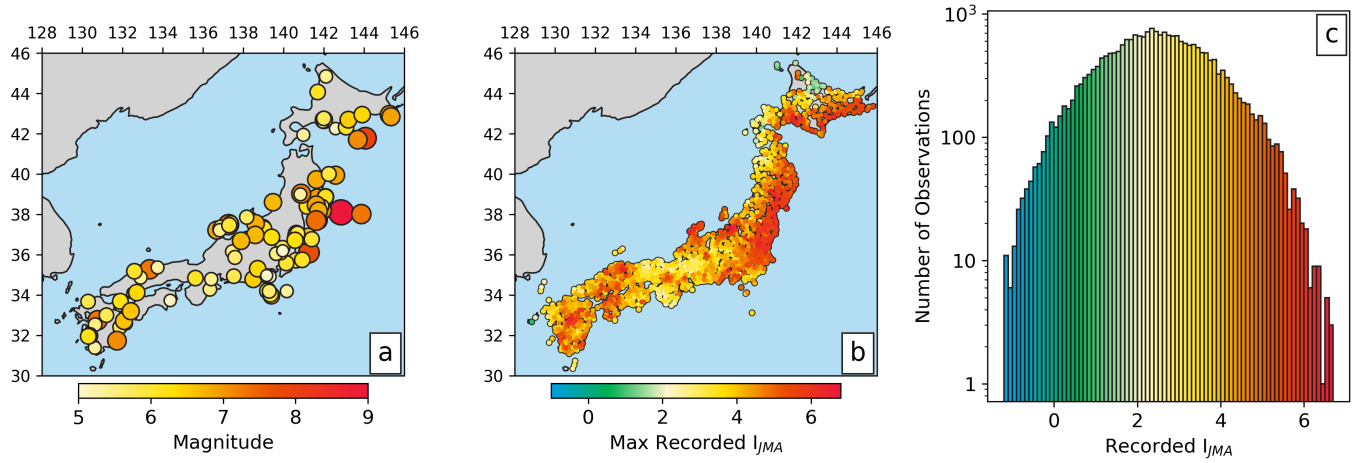


Figure 1 Locations and recorded intensities for 112 $\geq M_w$ 5.0 earthquakes between January 1997 and December 2025 that generate at least one recording $\geq$ 5.0 I_{JMA}. (a) Locations of processed earthquakes coloured and scaled by their respective magnitudes. (b) K-Net and KiK-net stations coloured by maximum recorded I_{JMA} value. (c) Histogram of observed I_{JMA} values within our ground motion intensity dataset.

puted from a_0 (in cm/s^2) using a logarithmic relationship:

$$I_{\text{JMA}} = 2\log_{10}(a_0) + 0.94. \tag{2}$$

Resulting I_{JMA} values are always reported to one decimal place and this calculation is performed using the *shindo.py* python library (RR-Inyo, 2021).

Peak ground acceleration (PGA) is the absolute maximum acceleration experienced at a location during an earthquake. Ground motion models typically report either the geometric mean (GM) of the horizontal components of shaking, or the median response when rotated over all horizontal orientations (RotD50; Boore, 2010). These measures are defined as

$$\text{PGA}_{\text{GM}} = \sqrt{\max_t |a_1(t)| \times \max_t |a_2(t)|} \tag{3}$$

and

$$\text{PGA}_{\text{RotD50}} = \text{median}_{\theta\in[0,\pi]} \left[\max_t |a_1(t)\cos\theta + a_2(t)\sin\theta| \right], \tag{4}$$

respectively, where a_1 and a_2 are recorded accelerations in two orthogonal horizonal directions as a function of time (t), and θ is the rotation angle between 0° and 180°.

Spectral acceleration ($S_a(T)$) is the maximum acceleration experienced by an idealised damped oscillator with a specified natural period of T seconds when subjected to ground motion. Typically, S_a is calculated assuming 5% damping and can be expressed at a range of periods including 0.2, 0.3, 0.6, 1.0, 2.0, and 3.0 s.

PGA and $S_a(T)$ values in RotD50, N-S, and E-W orientations used in this study are obtained from the open-source ground motion parameter flatfile for recordings from KiK-net and K-Net stations developed by Loviknes et al. (2026a,b). This database is generated using a comprehensive automated processing workflow. We only retain recordings classified as 'high quality' by Loviknes et al. (2026b), defined as a noise-energy ratio < 0.01, an acceptable frequency range ratio > 0.6, and a low chance of multiple-event contamination (signal energy ratio > 0.8). The geometric mean of PGA and $S_a(T)$ are computed following Equation 3. We report all PGA and $S_a(T)$ values in gal (equivalent to 1 cm/s^2 or 1/980.665 g). Our final database includes I_{JMA}, PGA, S_a(0.2 s), S_a(0.3 s), S_a(0.6 s), S_a(1.0 s), S_a(2.0 s), and S_a(3.0 s) observations for 21,354 strong motion recordings across 112 earthquakes (Figure 1b,c; Supplementary Table 1).

3 Regression Modelling

3.1 Methodology

Our aim is to develop parameterisations for I_{JMA} that are both accurate and simple to use within most insurance pricing workflows. As such, we opt for a regression

model and avoid more complex machine-learning approaches, as they often reduce interpretability and can be difficult to operationalise and audit. Since not all earthquake risk models provide the same ground motion parameters, we compute several alternative parameterisations to suit most users. The variables we investigate include M_w; the distance between the earthquake hypocentre and recording station (D_{hyp}); and strong ground motion intensities PGA, S_a(0.2 s), S_a(0.3 s), S_a(0.6 s), S_a(1.0 s), S_a(2.0 s), and S_a(3.0 s). Hypocentral distance and strong motion intensities are reported in km and gal, respectively. The relationship between I_{JMA} and maximum acceleration a_0 is log linear and several previous authors have identified log linear relationships between I_{JMA} and both D_{hyp} and ground motion intensities (Campbell and Bozorgnia, 2011; Karim and Yamazaki, 2002; Midorikawa et al., 1999). We therefore assume a regression with the form

$$\min \sum_{i=1}^{n} (y_i - \hat{y}_i)^2 \quad \text{where} \quad \hat{y}_i = b_0 + b_1 M_{wi} + \sum_{j=2}^{p} b_j \log_{10}(x_{ij}) \tag{5}$$

Here, regression coefficients $b_{(0\ldots p)}$ are estimated by minimising the squared error between observed and predicted I_{JMA} values (y_i and $\hat{y}_i$, respectively); x_{ij} where $j = 1$ is M_w and x_{ij} where $j > 1$ are D_{hyp} and strong ground motion intensities; and p is the total number of coefficients.

Parametric insurance contracts typically trigger at $I_{\text{JMA}} \geq 5.5$, where buildings begin to be materially damaged. However, accelerometer recordings that exceed this value only comprise 1.2% of the dataset, which is strongly skewed towards lower I_{JMA} values (see Figure 1c). We therefore apply a weighting approach to increase the influence of higher I_{JMA} values within our regression. I_{JMA} observations are weighted by the inverse of their respective count frequencies (f) within the dataset. To ensure our regression is optimised for I_{JMA} values that are relevant in an insurance context, this weight is multiplied by a scaling factor which linearly increases from 0 to 1 as I_{JMA} increases from ≤ 2 to ≥ 4.5. All weights (w) are normalised so that they have a mean of 1,

$$w_i = \frac{\frac{m(y_i)}{f(y_i)}}{\frac{1}{n}\sum_{j=1}^{n} \frac{m(y_j)}{f(y_j)}} \quad \text{where} \quad m(y) = \begin{cases} 0, & y \leq 2, \\ \dfrac{y-2}{2.5}, & 2 < y < 4.5, \\ 1, & y \geq 4.5 \end{cases} \tag{6}$$

Strong multicollinearity may exist between $\log_{10}$(PGA) and $\log_{10}(S_a(T))$ since these variables are all accelerations calculated from the same waveform. Furthermore, both M_w and D_{hyp} may also correlate with ground motion intensities since larger, closer earthquakes tend to cause greater shaking. Including two or more highly correlated variables within a regression increases the variance of their associated coefficients – making them more sensitive to changes in the underlying data, thereby increasing standard error. Figure 2a shows a matrix of Pearson correlation coefficients (R) between each variable and I_{JMA} for recordings where $I_{\text{JMA}} \geq 2$. All strong motion intensity variables show a positive correlation with I_{JMA} ($R \geq 0.7$). However, $\log_{10}$(PGA) and $\log_{10}(S_a(T))$ with periods between 0.2 s and 1 s are strongly correlated with each other ($R \geq 0.6$), as are periods between 1.0 s and 3.0 s ($R \geq 0.85$).

To mitigate multicollinearity, we employ a ridge regression approach (Hoerl and Kennard, 1970). Ridge regression applies a penalty function that forces coefficients towards zero, thereby reducing overfitting and model instability. All variables are standardised so that their contributions to the penalty function are equally weighted. The adapted regression equation is

$$\min \left(\sum_{i=1}^{n} w_i (y_i - \hat{y}_i)^2 + \lambda \sum_{j=1}^{p} b_{ij}^2 \right), \tag{7}$$

where b_j represents coefficients for all n variables and λ is the tuning parameter. As λ increases, coefficients are forced closer to zero, decreasing the variance in fit between subsets of sample data but reducing the goodness of fit to the subset of data provided. To select λ, we conduct a search where λ is varied between 0.1 and 1000 and select the λ that provides the lowest weighted root mean squared error (wRMSE) in a five-fold cross-validation exercise.

3.2 Regression Results

Our regression methodology is applied to all 511 possible variable combinations drawn from the nine parameters recorded in our database: M_w, D_{hyp}, PGA, S_a(0.2 s), S_a(0.3 s), S_a(0.6 s), S_a(1.0 s), S_a(2.0 s), and S_a(3.0 s). Regressions are computed for parameters derived from both geometric mean and RotD50 horizontal-component orientations, yielding a total of 1,022 candidate models. Resulting variable coefficients, regularisation parameters, and wRMSE for each model are reported in Supplementary Table 2.

In regression analysis, model fit improves as additional predictor variables are introduced. Akaike and Bayesian Information Criteria are typically calculated to identify the most parsimonious well-performing models; however, these metrics become less sensitive to changes in degrees of freedom as the number of samples exceeds a few thousand (Supplementary Table 2). Instead, we compare the wRMSE of all candidate models as a function of the number of included variables (Figure 2b).

Resultant parameterisations have wRMSEs ranging from 0.15–1.2 and cluster in two broad groups separated at approximately wRMSE ≈ 0.4. No models that have a wRMSE ≥ 0.4 include PGA or Sa(0.3 s) – the variables that most strongly correlate with I_{JMA} (Figure 2a). The

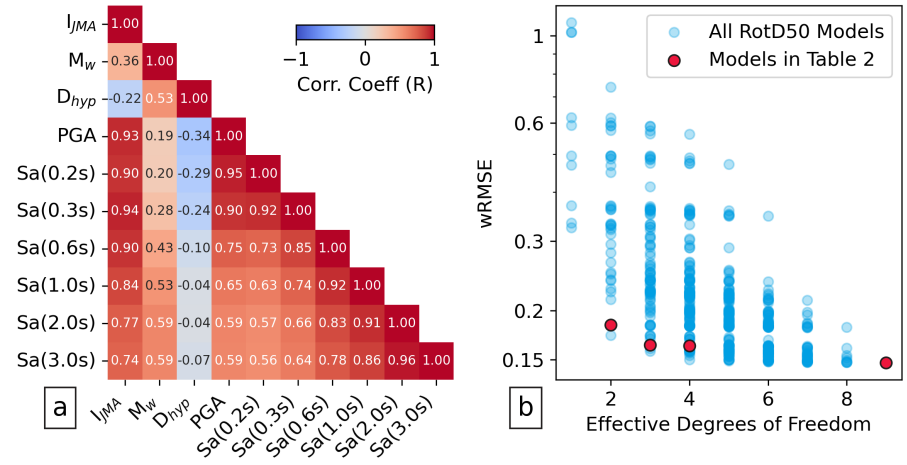


Figure 2 (a) Cross correlation matrix of earthquake observations with $I_{\text{JMA}} \geq 2$ from our earthquake catalogue (Supplementary Table 1). All ground motion intensities are presented as the RotD50 of their horizontal components. D_{hyp} and ground motion parameters are presented as the $\log_{10}()$ of their respective values. Each combination of variables is coloured and annotated with its respective Pearson correlation coefficient calculated using their respective absolute values. (b) Weighted root mean squared error (wRMSE) as a function of the number of variables in 511 possible regression parameterisations constructed from variables shown in Figure 2a. Blue circles = all parameterisations, red circle = best-fitting models detailed in Table 2.

Parameterisation	P1	P2	P3	P4	P5	P6	P7	P8
Variables	2	2	3	3	4	4	9	9
Orientation	GM	RotD50	GM	RotD50	GM	RotD50	GM	RotD50
λ	0.8	6.0	18.3	16.7	15.2	13.8	15.2	18.3
wRMSE	0.185971	0.183831	0.164390	0.163290	0.163930	0.162876	0.151019	0.147443
Intercept (b_0)	0.276927	0.302860	0.133852	0.159166	0.210278	0.231111	0.225841	0.263562
M_w					−0.013838	−0.013066	−0.0264228	−0.028766
$\log_{10}(D_{\text{hyp}})$							0.027517	0.032559
$\log_{10}(\text{PGA})$	1.383624	1.360097	0.935351	0.926618	0.926840	0.918698	0.921018	0.899983
$\log_{10}(S_a(0.2\,\text{s}))$							0.045087	0.048715
$\log_{10}(S_a(0.3\,\text{s}))$			0.513336	0.491639	0.522185	0.499956	0.334669	0.314437
$\log_{10}(S_a(0.6\,\text{s}))$							0.383164	0.40242
$\log_{10}(S_a(1.0\,\text{s}))$	0.680842	0.682945	0.597549	0.610601	0.607275	0.619713	0.274029	0.256567
$\log_{10}(S_a(2.0\,\text{s}))$							0.185456	0.190617
$\log_{10}(S_a(3.0\,\text{s}))$							−0.084618	−0.069448

Table 2 Each column details meta data and regression coefficients for a possible I_{JMA} parameterisation. Variables = number of variables used in the regression; orientations GM and RotD50 = ground motion intensities calculated as geometric mean and median response of horizontal components, respectively; λ = tuning parameter in ridge regression, wRMSE = weighted root mean squared error; all other values are regression coefficients for variables in the left-hand column.

best-performing models with 2, 3, 4, and 9 variables that do not rely on $S_a(0.6\,\text{s})$ or $S_a(3.0\,\text{s})$, which are less commonly calculated by earthquake risk models, are shown in Table 2. The best performing three-variable models achieve wRMSEs approaching that of the nine-variable model (0.1644 and 0.1633 for P3 and P4 versus 0.1510 and 0.1474 for P7 and P8, respectively; Figure 2b, Table 2). P3 and P4 employ PGA, $S_a(0.3\,\text{s})$, and $S_a(1.0\,\text{s})$, all of which are widely reported by ground motion models and the best-fitting four-variable solution that does not use $S_a(0.6\,\text{s})$ or $S_a(3.0\,\text{s})$ offers little improvement of fit (0.1639 and 0.1629, respectively; Figure 2b, Table 2). We therefore select P3 and P4 as our chosen parameterisations, which are respectively defined as

$$I_{\text{JMA}} = 0.133852 + 0.935351 \times \log_{10}(\text{PGA}_{\text{GM}}) + 0.513336 \times \log_{10}(S_a(0.3\,\text{s})_{\text{GM}}) + 0.597549 \times \log_{10}(S_a(1.0\,\text{s})_{\text{GM}}) \quad (8)$$

$$I_{\text{JMA}} = 0.159166 + 0.926618 \times \log_{10}(\text{PGA}_{\text{RotD50}}) + 0.491639 \times \log_{10}(S_a(0.3\,\text{s})_{\text{RotD50}}) + 0.610601 \times \log_{10}(S_a(1.0\,\text{s})_{\text{RotD50}}) \quad (9)$$

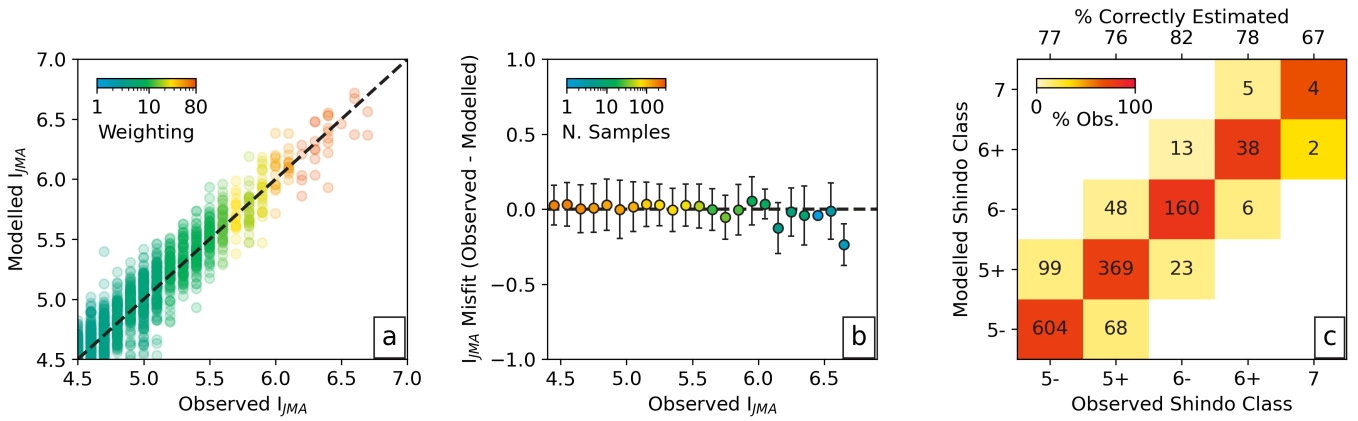


Figure 3 Comparison between observed and modelled I_{JMA} calculated using P4 in Table 2. (a) Modelled I_{JMA} as a function of observed I_{JMA} for all ground motions recordings with observed $I_{\text{JMA}} \geq 4.5$; samples coloured by weighting during regression fitting; dashed line = 1:1 for comparison. (b) Circles and error bars = mean and standard deviation residual misfit between observed and modelled I_{JMA} for all samples in each 0.1 I_{JMA} interval; circles coloured by the number of samples. (c) A comparison between observed and modelled Shindo classes using conversion outlined in Table 1. Number and colour of each bin denotes the count and percentage of observed samples of the class, respectively.

where all seismic intensities are in gal. Nevertheless, all possible solutions are included within Supplementary Table 2, so that users can identify their preferred model based on the variables available from their chosen ground motion or earthquake risk framework. Given the very similar performance of P3 and P4, we limit our analysis in the rest of the paper to P4 since we consider seismic intensity metrics described as RotD50 to currently be the most commonly used metric in ground motion modelling (e.g., Moschetti et al., 2024). The equivalent set of analyses for P3 are displayed in Supplementary Figures 1-4.

The performance of P4 at $I_{\text{JMA}} \geq 4.5$ is displayed in Figure 3. There is a strong overall agreement between observed and modelled I_{JMA} values with the majority of points clustering close to the 1:1 line (Figure 3a). Mean residuals for all I_{JMA} values ≤ 6.5 deviate < 0.15 from zero and have tight standard deviations (< 0.2), confirming the model is broadly unbiased (Figure 3b). Standard deviations are largest and a modest tendency towards underprediction is observed when $I_{\text{JMA}} \geq 6$. When I_{JMA} values are binned into Shindo Classes using the conversion illustrated in Table 1, we find that the model correctly identifies the class in 82% and 78% of cases where the observed Shindo classes are $6-$ and $6+$, respectively (Figure 3c). This classification rate reduces to 67% for a Shindo Class of 7, but this percentage is calculated using just six samples. Misclassifications are restricted to adjacent classes for all samples with an observed Shindo Class of $5+$ or greater.

4 Discussion

4.1 Comparison to an Established Parameterisation

To assess the performance of P4, we compare its predictive power to a commonly used published alternative by Karim and Yamazaki (2002); hereafter KY02. Several parametrisations are presented by KY02, but only Equation 14 in that paper does not rely on peak ground velocity or spectral intensity, and can therefore be implemented using the output from most contemporary earthquake risk models (such as the Global Earthquake Model; Fujiwara et al., 2023). Equation 14 in KY02 estimates that

$$I_{\text{JMA}} = -0.65 + 0.18 \times M_w + 1.81 \times \log_{10}(\text{PGA}_R), \quad (10)$$

where PGA_R is the maximum resultant horizontal PGA.

To compare the out-of-sample performance of P4 and KY02, we apply both to 256 recordings from the Next Generation Attenuation Subduction (NGA-Sub) database that occur outside of Japan, with a hypocentral depth ≤ 30 km, and yield a $\text{PGA}_{\text{RotD50}} \geq 0.1$ g (Supplementary Table 3; Mazzoni, 2022). For each recording, we calculate I_{JMA} from the raw accelerogram and take PGA and $S_a(T)$ values in RotD50 and GM orientation directly from the NGA-Sub database (Mazzoni et al., 2023). Figure 4a compares observed I_{JMA} values and those estimated using P4 this out-of-sample dataset. Most points lie close to the 1:1 line with a slight tendency to overestimate I_{JMA} in our out-of-sample data (see Figure 4b; wRMSE of 0.1963 using the weighting approach described in Equation 6). After converting I_{JMA} to Shindo Class, P4 correctly classifies 67% of out-of-sample recordings with a Shindo Class $\geq 6-$ (Figure 4c). In comparison, KY02 generates a broader scatter of I_{JMA} values around the 1:1 line with a higher wRMSE misfit, a strong bias to overestimate I_{JMA} values and this bias becomes more extreme at lower I_{JMA} values (0.4769; Figure 4d,e). These larger errors propagate into greater misclassifications of Shindo classes, with 54% of samples with a Shindo Class $\geq 6-$ correctly classified (Figure 4f). These biases are likely the result of a combination of differences in data recording, signal processing, and spectral composition of the earthquake waves used to generate these parameterisations. PGA can be sensitive to choices in low-pass filtering and noise reduction, which can be more consequential for records of less se-

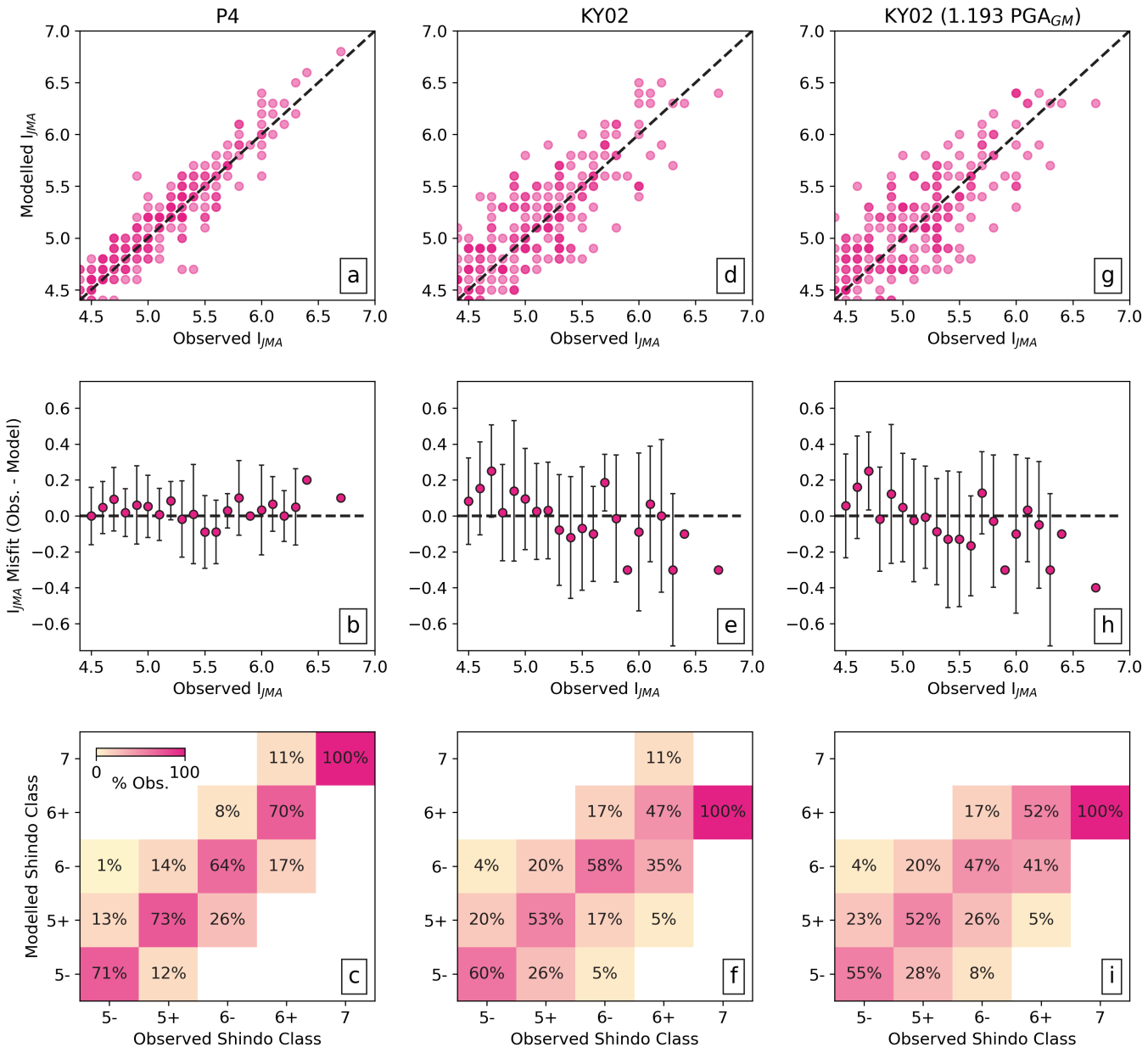


Figure 4 Comparison between observed and modelled I_{JMA} values using all non-Japanese accelerograms within the NGA-Subduction database with $\mathrm{PGA}_{\mathrm{RotD50}} \geq 0.1$ g (Supplementary Table 3 Mazzoni, 2022). (a) Modelled I_{JMA} as a function of observed I_{JMA} for all ground motions recordings with observed and modelled $I_{\mathrm{JMA}} \geq 4.5$. Dashed line = 1:1 for comparison. (b) Symbols and error bars = mean and standard deviation residual misfit between observed and modelled I_{JMA} for all samples in each 0.1 I_{JMA} interval. (c) A comparison between observed and modelled Shindo classes using conversion outlined in Table 1. Number and colour of each bin denotes percentage of observed samples of the class denoted by the X axis in the bin. (d-f) Same as 4a-c, respectively with I_{JMA} calculated using Equation 14 in Karim and Yamazaki (2002). (g-i) Same as 4d-f, respectively, using $\mathrm{PGA}_{\mathrm{GM}} \times 1.193$ in place of $\mathrm{PGA}_{\mathrm{R}}$.

vere shaking since they have a lower signal-to-noise ratio (Boore and Bommer, 2005). As a result, unfiltered records will have a higher PGA value, and the difference between unfiltered and filtered PGA values will increase as shaking decreases. Karim and Yamazaki (2002) do not discuss if/how their accelerograms have been filtered to account for noise. A less-severe or absent low-pass filtering of their accelerograms may explain the visible trend from over- to under-estimating I_{JMA} values as observed I_{JMA} increases (Figures 4e). NGA-Sub use a similar accelerogram filtering approach to NGA-West and NGA-East, which collectively underpin the earthquake ground motion prediction equations in the majority of modern earthquake risk models (e.g., Moschetti et al., 2024). The good performance of our parameterisation against this out-of-sample data suggests that it represents an improvement compared to KY02 for use on earthquake risk models.

A practical limitation of KY02 is that most earthquake risk models do not directly output PGA_R. Instead, they provide $\mathrm{PGA}_{\mathrm{GM}}$ or $\mathrm{PGA}_{\mathrm{RotD50}}$, and so an additional conversion step is typically required before KY02 can be applied. Karim and Yamazaki (2002) provide a conversion factor of 1.068 between PGA of the larger of the

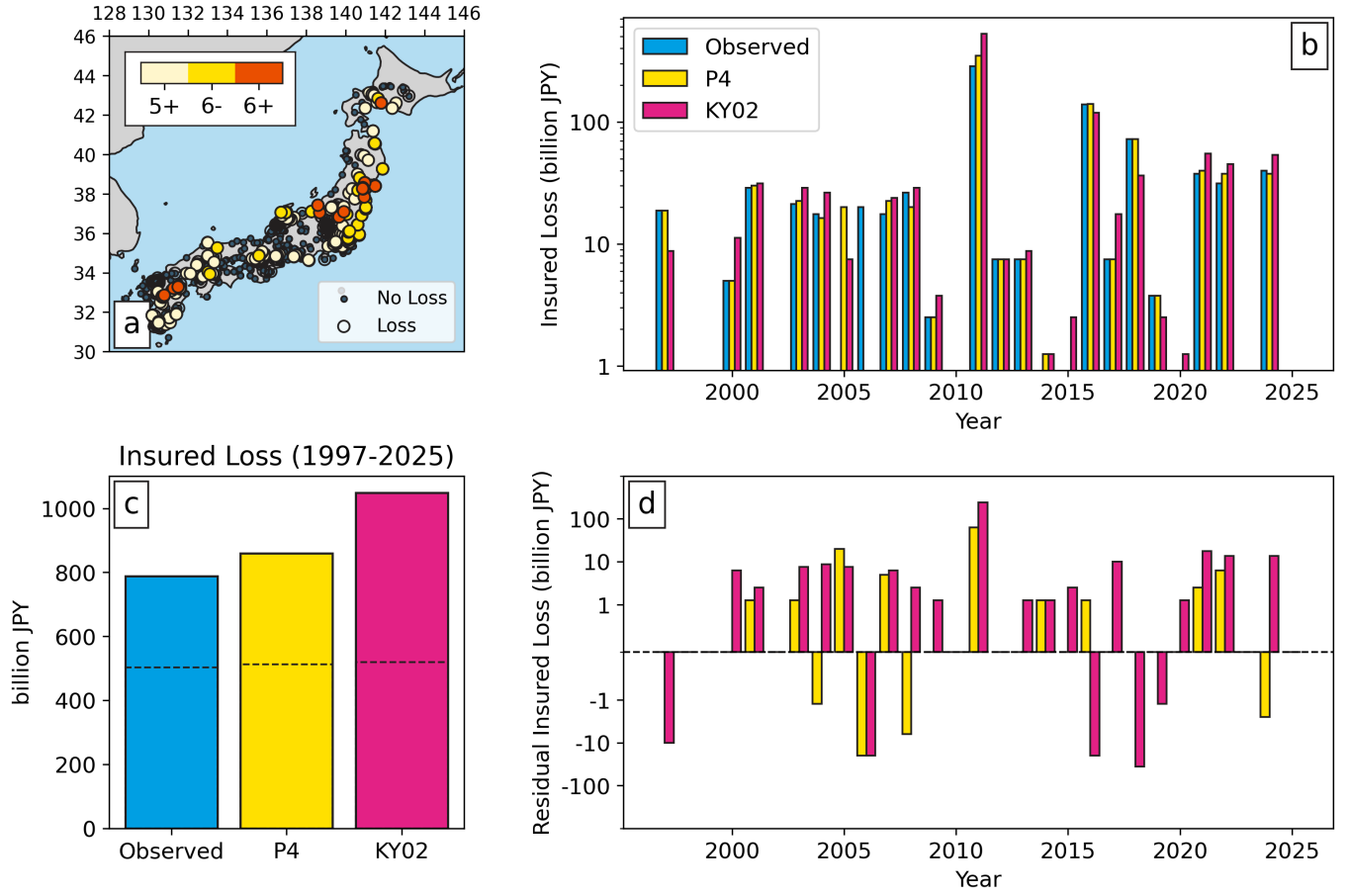


Figure 5 Application of I_{JMA} parameterisations to a synthetic parametric insurance portfolio using real events between 1997 and 2025. (a) Locations within the synthetic portfolio; small and large circles are untriggered and triggered locations, respectively (Supplementary Tables 1,4). Triggered locations coloured by the largest Shindo Scale experienced. (b) Loss experience time series; blue, yellow and pink bars show annual insured losses calculated using Shindo Class observations, those estimated using P4 and those calculated using KY02, respectively. (c) Aggregated losses for all events between 1997 and 2025; colours are the same as Figure 5b. Dashed line shows losses for all years except 2011. (d) Annual loss differences using Shindo Scale observations and parameterisation, positive values are parameterisation overestimates.

two horizontal coordinates (PGA_L) and PGA_R. Combining this PGA_L–PGA_R factor with a PGA_L–PGA_{GM} factor from Campbell and Bozorgnia (2007), yields a resultant conversion factor of 1.193. This value is similar to the mean conversion factor between PGA_R and PGA_{GM} for recordings with $I_{\text{JMA}} \geq 2$ in our Japanese ground motion dataset (1.194; Supplementary Table 1). Using this conversion elicits broadly similar results to using observed PGA_R values directly (wRMSE = 0.4770; Figure 4g–i). It is important to note that small differences in a conversion factor can strongly influence a parameterisation's performance – and published conversions can vary considerably (Shahi and Baker, 2014). These results demonstrate that parameterisations that require intermediate conversions of ground-motion terms can introduce potentially significant bias and uncertainty for I_{JMA} estimates that can have downstream impacts on basis risk and insurance decision making. These uncertainties must be considered and minimised in cases where a conversion is necessary.

4.2 Pricing an Illustrative Synthetic Insurance Portfolio

To demonstrate how uncertainties in I_{JMA} parameterisation propagate into insured losses, we apply observed and parameterised I_{JMA} observations between January 1997 and December 2025 to a synthetic parametric insurance portfolio. This synthetic portfolio combines healthcare facilities and power stations across Japan drawn from two publicly available datasets (Supplementary Table 4; Byers et al., 2018; Healthsites.io, 2026). Both asset classes serve critical social functions, have incurred losses during historic Japanese earthquakes, and could conceivably have parametric earthquake coverage (Kuo et al., 2004; Lipscy et al., 2013; Ohlmeyer et al., 2023; CCIRF SPC, 2025). By combining healthcare and power facilities, we hope to reflect the broad distribution of Japan's population and industry whilst providing reasonable coverage of its diverse earthquake risk and experience (Figure 5a).

We apply a parametric payout structure to each asset that attaches at a Shindo Class of 5+ and pays the full insured value if shaking reaches a Shindo Class of 7 (Table 3). This structure is reflective of existing formats

Shindo Class	5 Upper (5+)	6 Lower (6−)	6 Upper (6+)	7
I_{JMA}	$5.0 \leq I_{JMA} < 5.5$	$5.5 \leq I_{JMA} < 6.0$	$6.0 \leq I_{JMA} < 6.5$	$I_{JMA} \geq 6.5$
Payout (%)	12.5%	25%	50%	100%

Table 3 Parametric payout structure representing the percentage of the total insured value (10 billion JPY) that is paid to the insured in the event of an earthquake causing a Shindo intensity at or above the given thresholds at the nearest KiK-net or K-Net seismic station if one is located within 20 km at the time of the event.

in the market (Iwasaki, 2021; Descartes Underwriting, 2025). In each earthquake, every asset is assumed to experience the Shindo scale recorded at the closest K-Net or KiK-net station that was operational during the event, with a maximum seismometer-location distance of 20 km. All assets are allocated uniform insured values, or limits, of 10 billion JPY to create a 'flat portfolio' where limits are decoupled from true asset values. This normalisation removes confounding differences in underlying asset value and vulnerability to isolate the effect of I_{JMA} parameterisation. Note that the shaking experienced by the insured locations may differ from that of the seismic stations they are linked to; this additional basis risk is also present in real-world parametric insurance deals of this nature.

We subject our synthetic portfolio to all 112 historic earthquakes in our ground motion catalogue using observed I_{JMA} values, and those estimated using P4 and KY02. Total insured losses incurred by the synthetic portfolio each year using each I_{JMA} parameterisation are shown in Figure 5b. Losses calculated using observed intensities exceed 80 billion JPY in three major earthquake years: the 2011 Tōhoku-Oki, 2016 Kumamoto, and 2018 Osaka earthquakes. Together, these three years represent 64% of the 790 billion JPY total aggregate insured loss (Figure 5c). Both P4 and KY02 parameterisations overestimate aggregate losses compared to observations but the bias differs substantially (9% and 33%, respectively; Figure 5c). KY02 also generates larger, and more frequent annual residual losses, with annual loss misfits exceeding 10 billion JPY in 9 years compared to 3 years using P4 (Figure 5d). In a parametric insurance context, these discrepancies represent higher basis risk.

Aggregate loss overestimates for both parameterisations are primarily driven by the M_w 9.0 Tōhoku-Oki earthquake in 2011, the largest recorded earthquake and largest insurance loss in Japanese history (Figure 5d; Kajitani et al., 2013). If 2011 was removed from the loss history, P4 and KY02 overestimate losses by 1% and 3%, respectively (Figure 5c). Using P4 under- and overestimates losses in the Tōhoku earthquake for 11% and 18% of loss-paying locations, respectively (Figure 6a). Underestimated locations generally clustered around Tokyo Bay whilst overestimated locations occur around Tokyo Bay but also extend up into northern Kanto and Tōhoku. The same pattern is replicated in KY02, but shifted towards higher I_{JMA} values so that 55% of locations are overestimated (Figure 6b). Locations around Tokyo Bay are correctly or underestimated whilst the vast majority of locations that sit outside of Tokyo Bay are overestimated. These spatial and residual differences are likely attributable to variations in the treatment and abundance of data used to create each parameterisation, the extent to which each parameterisation captures local site conditions and their influence on ground motions, as well as the extreme magnitude and nature of the Tōhoku-Oki earthquake.

Both P4 and KY02 systematically overestimate I_{JMA} for the Tōhoku-Oki earthquake compared to other events with comparable I_{JMA} values (Figure 6c,d). For both parameterisations, this overestimation may be related to the extreme magnitude of the Tōhoku-Oki earthquake compared to other events used in parameterisation fitting. However, this effect is much more pronounced for KY02, which may stem from the inclusion of M_w as a direct additive within the parameterisation (Equation 10). Because M_w is an event-level property rather than a site-specific measure of shaking, its inclusion can introduce non-physical behaviour for large magnitude earthquakes or low levels of shaking. For example, if a station records no shaking for the Tōhoku-Oki earthquake, the KY02 parameterisation will estimate an I_{JMA} of ~1 solely due to the M_w term. This effect becomes more important for larger earthquakes with distal observations. P4 avoids this issue by relying exclusively on ground-motion intensity metrics, resulting in residual misfits for the Tōhoku-Oki earthquake that are much more tightly clustered around zero (Figure 6c).

Parameterisations of I_{JMA} that include peak ground velocity or spectral intensity terms generally outperform those based solely on PGA and M_w (Karim and Yamazaki, 2002; Midorikawa et al., 1999). Our results suggest that this improvement primarily reflects the inclusion of terms that respond to local site conditions, such as the stiffness of the subsurface. Near-surface stiffness is commonly quantified by the average shear-wave velocity within the top 30 m of the subsurface (V_{s30}). Softer sediments (i.e., lower V_{s30}) typically amplify seismic shaking as incoming shear waves decelerate as they enter lower stiffness materials. This amplification response varies considerably depending on the amplitude and frequency of incoming shear waves and the stiffness profile of the subsurface. During stronger shaking in soft sediments, higher frequency waves (e.g., S_a 0.1–0.3 s) can become increasingly damped whilst lower frequency waves (e.g., S_a 1.0–3.0 s) continue to amplify (Seyhan and Stewart, 2014). I_{JMA} is sensitive to a broad range of frequencies, whereas PGA is dominated by the highest-frequency components of shaking. Consequently, parameterisations that rely solely on PGA struggle to reproduce the full site response captured by I_{JMA}.

To evaluate this effect, we compare observed and parameterised I_{JMA} values for KiK-net recordings with

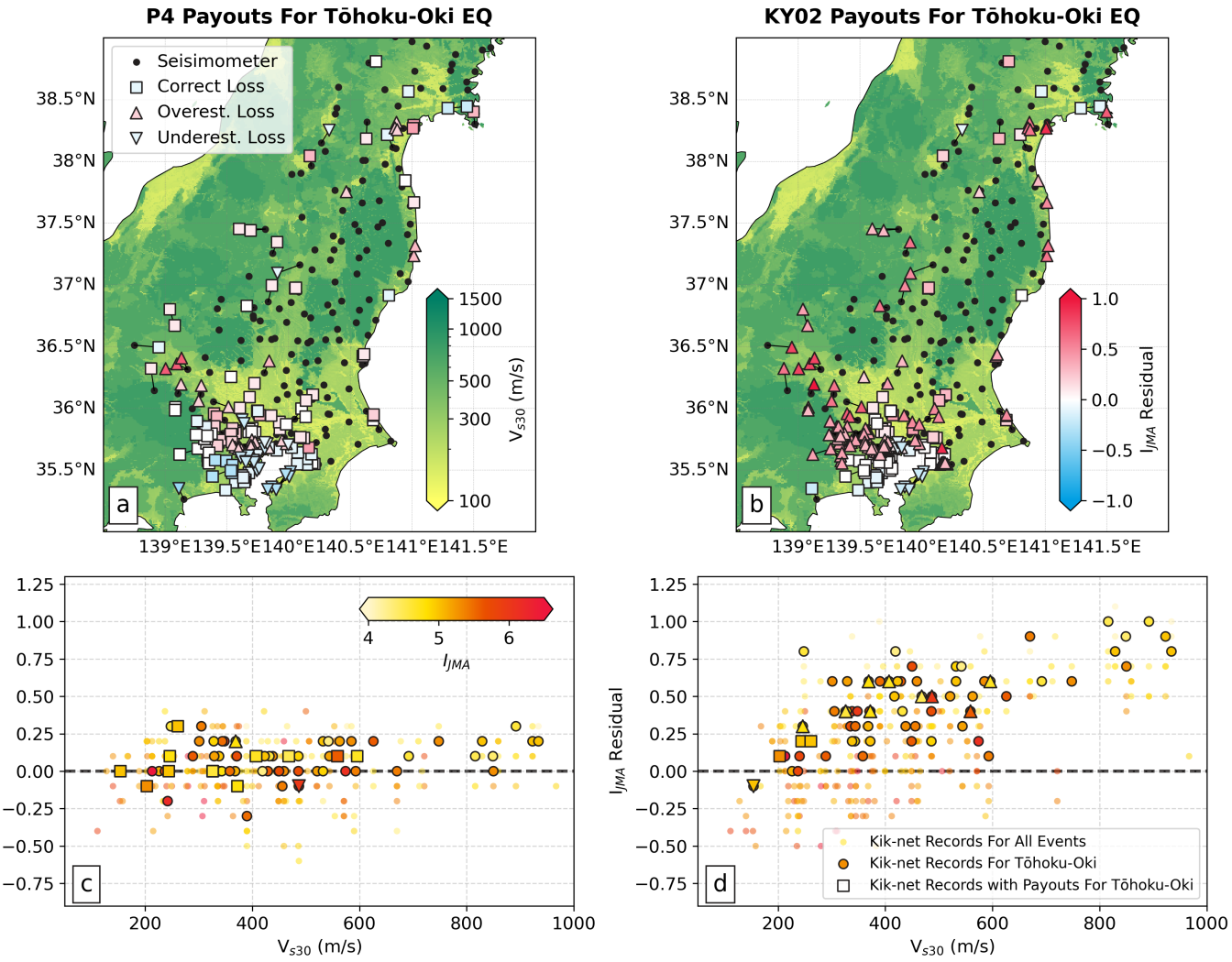


Figure 6 Parameterisation performance for the Tōhoku-Oki Earthquake, 2011. (a) Map of Tōhoku-Oki-earthquake-affected region with background grid coloured by shear-wave velocity in the top 30 m of the subsurface (V_{s30}; Heath et al., 2020). Inverted-triangles, squares, and triangles are insured locations where triggered losses in the synthetic portfolio are under-, correctly, and over-estimated using P4, respectively. Symbols are coloured by the residual misfit between parameterised and observed I_{JMA} and black lines tie insured locations to their nearest seismometer. Black dots are locations of seismometers with Tōhoku-Oki earthquake ground motion intensity recordings (Supplementary Table 1). (b) Same as Figure 6a with I_{JMA} values calculated using KY02. (c) Difference between observed and parameterised KiK-net station I_{JMA} values $\geq$ 4.5 using P4 in Table 2 as a function of V_{s30} values provided by Zhu et al. (2021). Small circles are all seismometer recordings for all earthquakes in Supplementary Table 1; large circles are recordings for Tōhoku-Oki earthquake; inverted-triangles/squares/triangles are recordings that trigger losses in the synthetic portfolio that are under-/correctly/over-estimated using P4. All symbols are coloured by their respective observed I_{JMA} values. (d) Same as Figure 6c but parameterised I_{JMA} calculated using Equation 14 in KY02.

$I_{\text{JMA}} \geq 4.5$ as a function of V_{s30} (Supplementary Table 1; Zhu et al., 2021). A slight positive correlation may be observed between V_{s30} and I_{JMA} calculated using P4 (Figure 6c). This correlation is much stronger for I_{JMA} calculated using KY02 for both the Tōhoku-Oki earthquake and the full observational record (Figure 6d). The overestimate of losses is significantly higher at stiffer, higher V_{s30} sites in the north and reduces in the softer sediment environment of Tokyo Bay. The inclusion of both PGA and S_a(1.0 s) terms in P4 better captures the combined influence of high- and low-frequency shaking on I_{JMA}. However, a slight increase in residual misfit remains at $V_{s30} \geq 600$ m/s since these two terms alone may not capture the full site response. Where practical, researchers may seek to use parameterisations in Supplementary Table 2 that include S_a(2.0 s) and S_a(3.0 s) terms, which may further reduce basis risk.

4.3 Implications for Future Parametric Insurance Contracts

Our I_{JMA} parameterisations reduce basis risk compared to KY02, so that underwriting and pricing teams can construct and evaluate I_{JMA}-based parametric policies with greater confidence. This new approach may encourage broader acceptance of such structures across both (re)insurance and insurance-linked securities markets, and support wider uptake of I_{JMA} as a principal trigger index. However, basis risk remains un-

avoidable when using parametric earthquake triggers. In practice, it arises from multiple sources including shaking differences between insured locations and reference seismometers and deviations between incurred damages and triggered payouts, as well as the uncertainties derived from the earthquake risk model used to price the contract. Nevertheless, basis risk can be mitigated by thoughtful payout-structure design (Calvet et al., 2017). For example, using 0.1 increments of I_{JMA} in place of steps in Shindo Class can mitigate thresholding effects and avoid large loss changes (e.g., Descartes Underwriting, 2025). Although increasing the number of steps can reduce the interpretability of the product, potential policy holders tend to prefer products that demonstrably reduce basis risk (Elabed et al., 2013). In addition, our simple synthetic example assumes that all hospitals and power plants have equal values and vulnerabilities. Detailed understanding of an asset's underlying risk (e.g., its structural vulnerability and historical damage) can improve the tailoring of an insurance policy and reduce basis risk.

Using I_{JMA} as a parametric insurance trigger introduces an additional modelling step compared to more common approaches such as PGA or M_w within a given distance. However, these simpler triggers can themselves produce substantial basis risk because they are poorer predictors of damage that do not adequately capture site amplification, shaking duration, and frequency-dependent effects (Wu et al., 2012; Montemayor et al., 2024). These issues are particularly important for structures on very soft or very stiff soils, or for buildings that are more vulnerable to lower-frequency shaking. The Modified Mercalli Intensity (MMI) scale offers a closer analogue to I_{JMA}, as it has been developed to reflect observed damage (Wald et al., 1999). However, MMI lacks instrumental objectivity, relying on observational reports in its derivation. Furthermore, PGA and MMI do not carry the same societal familiarity across Japan as I_{JMA}, which is embedded in public emergency broadcasting (Japan Meteorological Agency and Cabinet Office of Japan, 2004). As such, the close association between I_{JMA} and damage, its established meaning across Japanese society, and the objectivity of its calculation make it a beneficial trigger for both buyers and sellers of parametric earthquake products.

More broadly, the parametric insurance market would benefit from wider adoption of instrumentally-derived intensity metrics that incorporate multiple spectral frequencies and align more closely with observed damage. Beyond I_{JMA}, promising candidates include spectral intensity, average spectral acceleration, and filtered incremental velocity, which could serve as effective triggers in other seismic settings (Wu et al., 2012; Dávalos and Miranda, 2019; Monteiro et al., 2026). The methodology presented here provides a transferable framework for estimating any such metric from earthquake-model output, subject to the availability of sufficient observational data for calibration. Wider adoption of such indices could improve both the reliability and affordability of parametric earthquake (re)insurance globally — particularly in regions where large parametric policies serve as the primary financial protection for uninsured populations and public assets.

5 Conclusions

A suite of parameterisations has been constructed that estimate I_{JMA} from a variety of earthquake parameters and ground motion intensity metrics (Supplementary Table 2). These parameterisations are fitted to and evaluated with a large dataset of Japanese ground motion observations recorded between 1997 and 2025 (Supplementary Table 1). Of these, we select P3 and P4 in Table 2 as our most parsimonious well-fitting solutions and compare the performance of P4 to observed I_{JMA} values and those calculated using a previously published method (Karim and Yamazaki, 2002). We find P4 reduces misfit to observed I_{JMA} recordings compared to published approaches, particularly if users are constrained to the output of earthquake risk models. We believe these parameterisations will prove useful for both the earthquake risk and parametric insurance communities.

Acknowledgements

PWB and TS are supported by Inigo Insurance. We are grateful to A. Alvarez, T. Kang, L. Nicotina, R. Petrie, D. Smith, and A. Starr for their help. We thank NIED for recording and freely providing the seismic data used in this analysis (National Research Institute for Earth Science and Disaster Resilience, 2019). Figures were prepared using matplotlib (Hunter, 2007). We thank our two anonymous reviewers and the editor C. Galasso for their help to improve this manuscript.

Data and code availability

Processed seismic data and parameterisation results available in Supplementary Tables 1-4, respectively. All codes used in the creation of this paper are available at https://doi.org/10.5281/zenodo.20493491 (Ball and Sansom, 2026).

Competing interests

None

References

Aoi, S., Kunugi, T., and Fujiwara, H. Strong-motion seismograph network operated by NIED: K-NET and KiK-net. *Journal of Japan Association for Earthquake Engineering*, 4(3):65–74, 2004. doi: 10.5610/jaee.4.3_65.

Aoi, S., Kunugi, T., Nakamura, H., and Fujiwara, H. Deployment of new strong motion seismographs of K-NET and KiK-net. In *Earthquake Data in Engineering Seismology*, Geotechnical, Geological, and Earthquake Engineering, pages 167–186. Springer, Dordrecht, 2010. doi: 10.1007/978-94-007-0152-6_12.

Ball, P. and Sansom, T. paddywballinigo/Ball_Sansom_26: PS26_Submitted (PS26_Submitted). https://doi.org/110.5281/zenodo.20493491, 2026. Accessed: 2026-09-01.

Boore, D. M. Orientation-independent, nongeometric-mean measures of seismic intensity from two horizontal components of motion. *Bulletin of the Seismological Society of America*, 100(4): 1830–1835, 2010. doi: 10.1785/0120090400.

Boore, D. M. and Bommer, J. J. Processing of strong-motion accelerograms: needs, options and consequences. *Soil Dynamics and Earthquake Engineering*, 25(2):93–115, 2005.

Byers, L., Friedrich, J., Hennig, R., Kressig, A., Li, X., Malaguzzi Valeri, L., and McCormick, C. A Global Database of Power Plants. Technical note, World Resources Institute, 2018. https://www.wri.org/research/global-database-power-plants.

Calvet, L., Lopeman, M., de Armas, J., Franco, G., and Juan, A. A. Statistical and machine learning approaches for the minimization of trigger errors in earthquake catastrophe bonds. *Statistics and Operations Research Transactions*, pages 373–392, 2017. doi: 10.2436/20.8080.02.64.

Campbell, K. W. and Bozorgnia, Y. Campbell–Bozorgnia NGA ground motion relations for the geometric mean horizontal component of peak and spectral ground motion parameters. PEER Report 2007/02, Pacific Earthquake Engineering Research Center, 2007.

Campbell, K. W. and Bozorgnia, Y. A ground motion prediction equation for JMA instrumental seismic intensity for shallow crustal earthquakes in active tectonic regimes. *Earthquake Engineering & Structural Dynamics*, 40(4):413–427, 2011. doi: 10.1002/eqe.1027.

CCIRF SPC. Annual Report 2024-2025. Technical report, The Caribbean Catastrophe Risk Insurance Facility, 2025. https://www.ccrif.org/sites/default/files/publications/annualreports/CCRIF-SPC-Annual-Report-2024_2045_web.pdf.

Dávalos, H. and Miranda, E. Evaluation of the scaling factor bias influence on the probability of collapse using Sa(T1) as the intensity measure. *Earthquake Spectra*, 35(2):679–702, 2019.

Descartes Underwriting. Ensuring Resilience in Japan with Parametric Earthquake Solutions. https://descartesunderwriting.com/case-studies/ensuring-resilience-japan-parametric-earthquake-solutions, 2025. Accessed: 2026-05-26.

Earthquake Research Committee. Report: National Seismic Hazard Maps for Japan (2020) Map Edition. Technical report, Headquarters for Earthquake Research Promotion, 2021. https://www.jishin.go.jp/main/chousa/26jan_yosoku-e/index-e.htm.

Elabed, G., Bellemare, M. F., Carter, M. R., and Guirkinger, C. Managing basis risk with multiscale index insurance. *Agricultural Economics*, 44:419–431, 2013. doi: 10.1111/agec.12025.

Fujimoto, K. and Midorikawa, S. Empirical relationship between JMA instrumental seismic intensity and ground motion parameters considering the effect of earthquake magnitude. *Journal of Japan Association for Earthquake Engineering*, 10(2):1–11, 2010. doi: 10.5610/jaee.10.2_1.

Fujiwara, H., Morikawa, N., Maeda, T., Iwaki, A., Senna, S., Kawai, S., Azuma, H., Hao, X., Imoto, M., Wakamatsu, K., Miyakoshi, J., Morii, T., Shimazu, N., Takahashi, M., and Akatsuka, M. PSHA input model documentation for Japan (JPN). Technical report, Global Earthquake Model, 2023.

Härdle, W. K. and Cabrera, B. L. Calibrating CAT bonds for Mexican earthquakes. *Journal of Risk & Insurance*, 77(3):625–650, 2010. doi: 10.1111/j.1539-6975.2010.01355.x.

Healthsites.io. The Global Healthsites Mapping Project. https://healthsites.io/, 2026. Open healthcare facility dataset and API. Accessed: 2026-05-29.

Heath, D. C., Wald, D. J., Worden, C. B., Thompson, E. M., and Smoczyk, G. M. A global hybrid V_{S30} map with a topographic slope-based default and regional map insets. *Earthquake Spectra*, 36(3):1570–1584, 2020. doi: 10.1177/8755293020911137.

Hirono, T. and Sato, K. MSK intensity scale as compared with JMA intensity scale. *Papers in Meteorology and Geophysics*, 22(3–4): 177–193, 1971. doi: 10.2467/mripapers1950.22.3-4_177.

Hoerl, A. E. and Kennard, R. W. Ridge regression: Applications to nonorthogonal problems. *Technometrics*, 12(1):69–82, 1970. doi: 10.1080/00401706.1970.10488646.

Hunter, J. D. Matplotlib: A 2D graphics environment. *Computing in Science & Engineering*, 9(3):90–95, 2007. doi: 10.1109/MCSE.2007.55.

Iwasaki, M. Customer case study: Parametric QUAKE Japan. https://corporatesolutions.swissre.com/insights/knowledge/customer-case-study-parametric-quake-japan.html, 2021. Accessed: 2026-04-30.

Japan Meteorological Agency and Cabinet Office of Japan. On the Launch of the Estimated Seismic Intensity Distribution Map Service. Technical report, Japan Meteorological Agency, February 2004. https://www.jma.go.jp/jma/press/0402/26a/sindo040226.pdf. Press release. Accessed: 2025.

Kajitani, Y., Chang, S. E., and Tatano, H. Economic impacts of the 2011 Tohoku-Oki earthquake and tsunami. *Earthquake Spectra*, 29(S1):457–478, 2013. doi: 10.1193/1.4000108.

Karim, K. R. and Yamazaki, F. Correlation of JMA instrumental seismic intensity with strong motion parameters. *Earthquake Engineering & Structural Dynamics*, 31(5):1191–1212, 2002. doi: 10.1002/eqe.158.

Kiyono, J., Fujie, K., and Ohta, Y. A combined instrumental seismic intensity – concept, formulation and application. *Doboku Gakkai Ronbunshu*, 612:143–151, 1999.

Kuo, K., Hayashi, Y., and Kambara, H. Relationship between damages of hospital facilities and seismic intensity based on questionnaire survey. *J. Struct. Constr. Eng. AIJ*, 586:63–69, 2004. doi: 10.3130/aijs.69.63_6.

Lipscy, P. Y., Kushida, K. E., and Incerti, T. The Fukushima disaster and Japan's nuclear plant vulnerability in comparative perspective. *Environmental science & technology*, 47(12):6082–6088, 2013. doi: 10.1021/es4004813.

Loviknes, K., Von Specht, S., Lilienkamp, H., Händel, A., Zhu, C., and Cotton, F. KiK-net and K-NET flatfile with automatically processed ground motions and associated metadata V. 0002. Technical report, GFZ Data Service, 2026a. https://doi.org/10.5880/GFZ.LKUT.2026.003.

Loviknes, K., Von Specht, S., Lilienkamp, H., Händel, A., Zhu, C., and Cotton, F. Harmonization of KiK-net and K-NET Ground-Motion Parameters and Metadata: A Flatfile of 950,000 Three-Component Records Spanning 29 Years. *Seismica*, 5(1), 2026b.

Mazzoni, S. NGA-subduction portal: Ground-motion record selection and download. Technical report, The B. John Garrick Institute for the Risk Sciences, 2022. doi: 10.34948/N3D59V.

Mazzoni, S., Kishida, T., and Bozorgnia, Y. NGA-Subduction Component PSA IM Tables: H1, H2, V, RotD50, rotD100 5Damping R230104. Technical report, The B. John Garrick Institute for the Risk Sciences, 2023. doi: 10.34948/N3MS3N.

Midorikawa, S., Fujimoto, K., and Muramatsu, I. Correlation of new J.M.A. instrumental seismic intensity with former J.M.A. seismic intensity and ground motion parameters. *Journal of the Institute of Social Safety Science*, 1:51–56, 1999.

Mistry, H. K. and Lombardi, D. Pricing risk-based catastrophe bonds for earthquakes at an urban scale. *Scientific Reports*, 12: 9729, 2022. doi: 10.1038/s41598-022-13588-1.

Monteiro, V. A., Aristeidou, S., and O'Reilly, G. J. Spatial Cross-Correlation Models for Next-Generation Amplitude and Cumu-

lative Intensity Measures. *Earthquake Spectra*, 42(2):e70076, 2026.

Montemayor, D., Dávalos, H., and Miranda, E. Influence of ground motion duration on collapse risk: spectral shape-amplitude scaling joint effects. In *The 18th World Conference on Earthquake Engineering*, pages 0–10, 2024.

Moschetti, M. P., Aagaard, B. T., Ahdi, S. K., Altekruse, J., Boyd, O. S., Frankel, A. D., Herrick, J., Petersen, M. D., Powers, P. M., Rezaeian, S., et al. The 2023 US national seismic hazard model: Ground-motion characterization for the conterminous United States. *Earthquake Spectra*, 40(2):1158–1190, 2024.

National Research Institute for Earth Science and Disaster Resilience. K-NET, KiK-net. Dataset, 2019. doi: 10.17598/NIED.0004.

Ohlmeyer, O., Hotz, M., and Martin, A. Parametric enables Nepal's renewable energy project financing. https://corporatesolutions.swissre.com/insights/knowledge/parametric-renewable-energy-nepal.html, 2023. Accessed: 2026-05-26.

Pavel, F. and Aldea, A. I_{JMA}-based evaluation of ground motion recordings from Vrancea intermediate-depth earthquakes. *Bulletin of Earthquake Engineering*, 23:4285–4303, 2025. doi: 10.1007/s10518-025-02220-y.

Rao, A., Yepes-Estrada, C., Johnson, K., Todorović, L., Pagani, M., Simionato, M., Styron, R., Silva, V., and Crowley, H. Evolution of the OpenQuake Engine: Enhanced capabilities, collaborative development, and global adoption. *Earthquake Spectra*, 41(5): 3299–3336, 2025.

RR-Inyo. shindo: Calculates JMA (Japan Meteorological Agency) Seismic Intensity (Shindo) Scale from Acceleration Data Recorded in NumPy Array. https://github.com/RR-Inyo/shindo, 2021. https://github.com/RR-Inyo/shindo. Accessed: 2026-06-01.

Seyhan, E. and Stewart, J. P. Semi-empirical nonlinear site amplification from NGA-West2 data and simulations. *Earthquake Spectra*, 30(3):1241–1256, 2014. doi: 10.1016/j.soildyn.2014.08.015.

Shahi, S. K. and Baker, J. W. NGA-West2 models for ground motion directionality. *Earthquake Spectra*, 30(3):1285–1300, 2014.

Silva, V., Amo-Oduro, D., Calderon, A., Costa, C., Dabbeek, J., Despotaki, V., Martins, L., Pagani, M., Rao, A., Simionato, M., Viganò, D., Yepes-Estrada, C., Acevedo, A., Crowley, H., Horspool, N., Jaiswal, K., Journeay, M., and Pittore, M. Development of a global seismic risk model. *Earthquake Spectra*, 36(1):372–394, 2020. doi: 10.1177/8755293019899953.

Wald, D. and Franco, G. Financial decision-making based on near-real-time earthquake information. In *Proceedings of the 16th world conference on earthquake engineering*, pages 1–13. Santiago de Chile Chile, 2017. http://www.wcee.nicee.org/wcee/article/16WCEE/WCEE2017-3625.pdf.

Wald, D. J., Quitoriano, V., Heaton, T. H., and Kanamori, H. Relationships between peak ground acceleration, peak ground velocity, and modified Mercalli intensity in California. *Earthquake spectra*, 15(3):557–564, 1999.

Willard, J. HDI Global SE & Descartes receive approval to provide parametric earthquake insurance in Japan. https://www.artemis.bm/news/hdi-global-se-descartes-receive-approval-to-provide-parametric-earthquake-insurance-in-japan.html, 2025. Accessed: 2026-04-30.

Wu, H., Masaki, K., Irikura, K., Saguchi, K., Kurahashi, S., and Wang, X. Relationship between building damage ratios and ground motion characteristics during the 2011 Tohoku Earthquake. *Journal of Natural Disaster Science*, 34(1):59–78, 2012.

Zhu, C., Weatherill, G., Cotton, F., Pilz, M., Kwak, D. Y., and Kawase, H. An open-source site database of strong-motion stations in Japan: K-NET and KiK-net (v1. 0.0). *Earthquake Spectra*, 37(3): 2126–2149, 2021.

The article *Empirical Relationships Between Ground Motion Intensities and JMA Seismic Intensity Scale* © 2026 by Patrick W. Ball is licensed under CC BY 4.0.